

Proton NMR study of spin dynamics in the magnetic organic chains $M(\text{hfac})_3\text{NITet}$ ($M = \text{Eu}^{3+}, \text{Gd}^{3+}$)

M. Mariani,^{1,2} A. Lascialfari,^{3,1,4,*} A. Caneschi,⁵ L. Ammannato,⁵ D. Gatteschi,⁵ A. Rettori,^{6,4} M. G. Pini,⁷
C. Cucci,⁸ and F. Borsa^{1,9}

¹Dipartimento di Fisica, Università degli Studi di Pavia and INSTM, I-27100 Pavia, Italy

²Dipartimento di Fisica, Università degli Studi di Bologna, I-40127 Bologna, Italy

³Dipartimento di Fisica, Università degli Studi di Milano and INSTM, I-20133 Milano, Italy

⁴Centro S3, c/o Istituto Nanoscienze del CNR (CNR-NANO), I-41125 Modena, Italy

⁵Dipartimento di Chimica, Università degli Studi di Firenze, and INSTM, I-50019 Sesto Fiorentino (FI), Italy

⁶Dipartimento di Fisica ed Astronomia, Università di Firenze, I-50019 Sesto Fiorentino (FI), Italy

⁷Istituto dei Sistemi Complessi del CNR (CNR-ISC), Unità di Firenze, I-50019 Sesto Fiorentino (FI), Italy

⁸Institute of Applied Physics “Nello Carrara”, Italian National Research Council (CNR-IFAC), I-50019 Sesto Fiorentino (FI), Italy

⁹Department of Physics and Astronomy and Ames Laboratory, Iowa State University, Ames, Iowa 50011, USA

(Received 22 May 2015; revised manuscript received 5 November 2015; published 11 April 2016)

In this work, we present a nuclear magnetic resonance (NMR) study of the spin dynamics in the rare-earth-based low-dimensional molecular magnetic chains $\text{Eu}(\text{hfac})_3\text{NITet}$ and $\text{Gd}(\text{hfac})_3\text{NITet}$ (in short, Eu-Et and Gd-Et). Although both samples are based on the same chemical building block, $[(\text{hfac})_3\text{NITet}]$, their magnetic properties change dramatically when the Eu^{3+} ion, which is nonmagnetic at low temperatures, is substituted by the magnetic Gd^{3+} ion. The present proton NMR investigation shows that, down to the lowest investigated temperature ($T = 1.5$ K for Gd-Et and $T = 3$ K for Eu-Et), the Eu-Et chain behaves as a one-dimensional Heisenberg model with antiferromagnetic exchange coupling ($J = -20$ K) between $s = 1/2$ organic radicals, and has a T -independent exchange frequency ($\omega_e = 2.6 \times 10^{12}$ rad/s). In the Gd-Et chain, in contrast, a competition arises between nearest-neighbor ferromagnetic coupling and next-nearest-neighbor antiferromagnetic coupling; moreover, two phase transitions have previously been found, in agreement with Villain’s conjecture: a first transition, at $T_0 = 2.2$ K, from a high temperature paramagnetic phase to a chiral spin liquid phase, and a second transition, at $T_N = 1.9$ K, to a three-dimensional helical spin solid phase. Contrary to the Eu-Et chain (whose three-dimensional ordering temperature is estimated to insurge at very low, $T_N \approx 0.3$ K), critical spin dynamics effects have been measured in the Gd-Et chain on approaching $T_N = 1.9$ K: namely, a divergence of the proton nuclear spin-lattice relaxation rate $1/T_1$, which in turn produces a sudden wipe-out of the NMR signal in a very narrow ($\Delta T \sim 0.04$ K) temperature range above T_N . Below T_N , an inhomogeneous broadening of the NMR line indicates a complete spin freezing. At $T_0 = 2.2$ K, instead, such critical effects are not observed because NMR measurements probe the two-spin correlation function, while the chiral spin liquid phase transition is associated with a divergence of the four-spin correlation function.

DOI: [10.1103/PhysRevB.93.134410](https://doi.org/10.1103/PhysRevB.93.134410)

I. INTRODUCTION

In the last decades, it has been possible to synthesize organic molecules which incorporate magnetic ions and free radicals, resulting in quasi-one-dimensional (1D) magnetic chains with very interesting properties [1–7]. One of these new classes of compounds is characterized by the regular alternation of magnetic centers (M) and nitronyl-nitroxide organic radicals (NITR) along a certain crystallographic direction. The properties of the resulting magnetic chain can be tuned by changing the magnetic ion M , and/or R in the organic radical (with the formula $\text{NITR} = 2\text{-R-4,4,5,5-tetramethyl-4,5-dihydro-1H-imidazolyl-1-oxyl 3-oxide}$). M can be a transition-metal (TM) or a rare-earth (RE) ion [8–10], while in NITR possible choices are $R = \text{ethyl (Et), isopropyl (iPr), methyl (Me), or phenyl (Ph)}$. The case where the magnetic ion is a rare earth assumes a particular interest, because the ground state can range from nonmagnetic ($M = \text{Eu}^{3+}, \text{Y}^{3+}$) to isotropic ($M = \text{Gd}^{3+}$) to strongly anisotropic ($M = \text{Dy}^{3+}$) [8,11]. Furthermore, by

inserting different radicals R in a rare-earth-based chain, one can obtain a family of quasi-1D helimagnets, $M(\text{hfac})_3\text{NITR}$ ($\text{hfac} = \text{hexafluoroacetylacetonate}$), with different degrees of frustration arising from the competing intrachain magnetic interactions between nearest-neighbor (nn) and next-nearest-neighbor (nnn) magnetic centers [12–18]. Several papers have been devoted to the investigation of the magnetic phase transitions [12–19] in such chains with different RE ions and radical groups. However, a detailed study of the spin dynamics is still lacking. Local spectroscopic probes like nuclear magnetic resonance (NMR) are particularly appealing to this aim, since they can provide useful information on the mechanism of the transition in the neighborhood of the critical temperature, where the onset of magnetic order occurs. When applied to hydrogen nuclei, present in great abundance in the organic magnetic chains, the NMR technique appears to be well suited to study the electronic spin dynamics [20]. The protons are coupled by dipolar and/or hyperfine interactions to the magnetic (electronic) centers. Thus, freezing of the electronic spins at phase transitions results in an inhomogeneous broadening and appearance of a hyperfine structure in the proton NMR line, while the critical slowing down of the magnetic

*alessandro.lascialfari@unimi.it

spin fluctuations can induce a critical enhancement of the proton spin-lattice and spin-spin relaxation rates [20,21]. With the aim of highlighting such effects on experimental NMR quantities, we chose to investigate the quasi-one-dimensional helimagnet $\text{Gd}(\text{hfac})_3\text{NITet}$, for which a rich phenomenology is present at low temperature [12–15,18]. For the purpose of having a reference compound isomorphous to the Gd chain, but without a magnetic RE ion, we have also investigated the system $\text{Eu}(\text{hfac})_3\text{NITet}$. In fact, the replacement of the magnetic Gd^{3+} RE ion, with $S = 7/2$, by the Eu^{3+} RE ion, which is nonmagnetic at low T , reduces the system to a simple Heisenberg chain of organic radical magnetic centers, with $s = 1/2$.

II. EXPERIMENTAL DETAILS

The two investigated molecular magnetic chains, $M(\text{hfac})_3\text{NITet}$, with $M = \text{Gd}^{3+}$ and Eu^{3+} , were found to be isomorphous and isostructural [19,22]. The coordination number for the magnetic center is eight, counting the two oxygen atoms of the two nitronyl-nitroxides and the six oxygen atoms of the three hfac moieties. The bridges of the metal ions are composed of NITet, characterized by two N-O groups which share one electron. This ensures a strong transmission of the interaction along the chain. In these compounds, where the chains develop along the crystallographic c axis, the unit cell is monoclinic, with two slightly different Gd environments [19]. The details of the synthesis and structural characterization are described elsewhere [8,22]. The scheme of the Gd-chain structure is reported in Fig. 1, where the exchange interactions responsible for the magnetic properties of the system are also sketched [see Eq. (8) below]. The scheme of the different magnetic phases of $\text{Gd}(\text{hfac})_3\text{NITet}$, predicted by Villain years ago [23], is reported in Fig. 2 and briefly discussed later on. In the Eu chain, as anticipated, the Eu^{3+} ion, which is nonmagnetic at very low temperatures, is put in place of the Gd^{3+} one, and just the radical-radical exchange coupling is present.

Magnetic measurements were performed on powder samples with a Quantum Design MPMS-XL7 magnetometer. The zero-field cooled and field-cooled magnetization curves vs temperature have been collected from 2 to 300 K. In order to understand the effect of the magnetic field on the ordering of the spin ensemble, the measurements for the Gd chain have been performed at several applied fields, from $H = 0.001$ up to 0.3 Tesla, while for the Eu chain the measurements were taken only at $H = 0.1$ Tesla. For low fields, one has that the measured quantity M/H approximately corresponds to the magnetic susceptibility χ , while for higher fields nonlinear effects come into play. This may explain the qualitatively different behavior of M/H in the Gd chain for $H = 0.001$ T with respect to M/H for higher values of the applied field (see Fig. 6 later on).

The ^1H NMR measurements were performed on powder samples, by means of pulsed FT Apollo-Tecmag and Stellar-Spinmaster spectrometers. NMR spectra were obtained from the Fourier transform of half of the echo signal in the case the entire linewidth was irradiated by the excitation radiofrequency pulse, while the wider spectra were collected taking the envelope of the Fourier transforms at different frequencies,

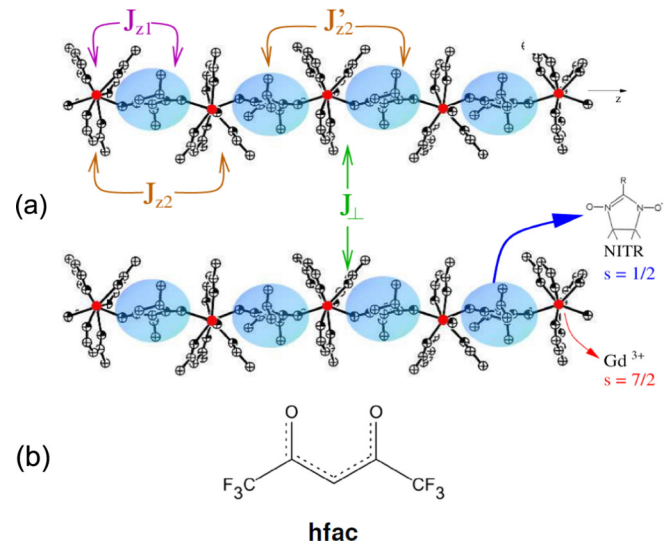


FIG. 1. (a) Scheme of the investigated $\text{Gd}(\text{hfac})_3\text{NITet}$ molecular magnetic chain. $J_{z1} = 5.05$ K is the intrachain nearest-neighbor (nn) ferromagnetic exchange constant between Gd^{3+} ions ($S = 7/2$) and radicals ($s = 1/2$); $J_{z2} = -0.98$ K is the intrachain next nn antiferromagnetic exchange coupling between Gd^{3+} ions; $J'_{z2} = -7.67$ K is the intrachain next nn antiferromagnetic exchange coupling between radicals; $J_{\perp} \ll J_{z1}$ is the interchain exchange coupling. The schematic view of NITet ($R = \text{Et}$) group is also reported. (b) The moiety hfac. The $\text{Eu}(\text{hfac})_3\text{NITet}$ molecular magnetic chain is isostructural with $\text{Gd}(\text{hfac})_3\text{NITet}$: In place of the magnetic RE ion Gd^{3+} , it has the RE ion Eu^{3+} , which is nonmagnetic at low temperature.

around the Larmor frequency, by sweeping the frequency itself and keeping the magnetic field constant. The spin-spin relaxation time T_2 was measured by the Hahn echo pulse sequence $(\pi/2)_x - \pi_y$, while for the spin-lattice relaxation time T_1 we used the same reading sequence, but with a saturating comb of 10–20 pulses applied at a variable delay time before the Hahn echo couple of pulses. The length of the $\pi/2$ pulse was in the range 2.3–3.1 μs , slightly increasing at higher

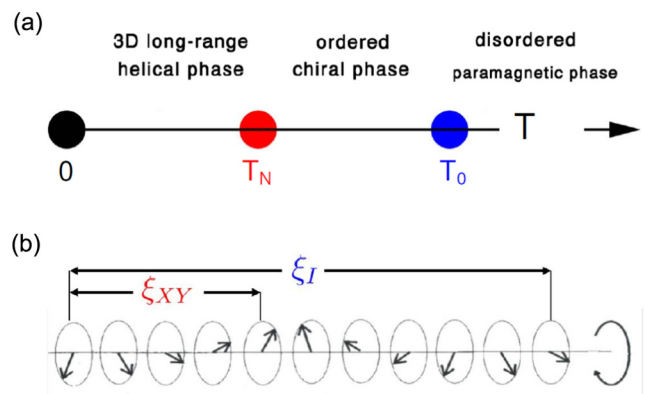


FIG. 2. (a) Scheme of the phase diagram of $\text{Gd}(\text{hfac})_3\text{NITet}$, with a chiral phase transition at $T_0 = 2.2$ K, and a helical phase transition at $T_N = 1.9$ K. (b) Graphical representation of the correlation lengths in the 3D long-range helical phase ξ_{XY} , and in the ordered chiral phase ξ_I .

resonance frequency. The relaxation curve of the transverse nuclear magnetization resulted in being single exponential, and T_2 was obtained by a simple fit to an exponential function. Instead, the recovery curves for the nuclear longitudinal magnetization presented a multiexponential behavior (as in other molecular magnets [20]), due to the existence of many inequivalent hydrogen sites. As a consequence, we chose to fit the data for $[M_z(t) - M_z(0)]/M_z(0)$ with the sum of two functions: (i) a dominating, fast-relaxing function that has a single exponential behavior $\exp[-(t/T_{1,\text{fast}})]$, except for the Gd-Et chain in the temperature range $2 < T < 6$ K, where it assumes a stretched exponential behavior $\exp[-(t/T_{1,\text{fast}})^\beta]$, with the free parameter β taking values comprised in the range $0.8 < \beta \leq 1$; (ii) a slow-relaxing exponential function $\exp[-(t/T_{1,\text{slow}})]$, with a low percent weight over the total magnetization (7%–19%, depending on temperature and the wipe-out entity), except for the Gd-Et chain in the temperature range $2 < T < 6$ K, where it assumes as well a stretched exponential behavior $\exp[-(t/T_{1,\text{slow}})^{\beta'}]$, with a different exponent $\beta' = 0.5$. The T_1 values reported in the following data discussion are the ones obtained from the fast-relaxing function, and pertain to hydrogen nuclei in proximity to the magnetic ions. The T_1 values associated with the slow-relaxing exponential do not reflect the electron spin dynamics, as they are attributed to hydrogen nuclei very weakly coupled to the magnetic ions.

III. RESULTS IN THE EUROPIUM CHAIN

Among the various molecular magnetic chains of formula $M(\text{hfac})_3\text{NITet}$, which are isomorphous and isostructural with the one containing $M = \text{Gd}^{3+}$, it is worth mentioning the compounds with $M = \text{Y}^{3+}$ and $M = \text{Eu}^{3+}$, which both have a nonmagnetic ground state. However, Y^{3+} is diamagnetic, while Eu^{3+} has magnetic excited states. Therefore, while the molecular magnetic chain $\text{Y}(\text{hfac})_3\text{NITet}$ can be described by a simple Heisenberg $s = 1/2$ antiferromagnetic model [8], whose properties are well known [24], the $\text{Eu}(\text{hfac})_3\text{NITet}$ chain is expected to have a more complicated behavior. In fact, even though the Eu^{3+} ions do not interact via a next-nearest-neighbor exchange (as the Gd^{3+} ions do in $\text{Gd}(\text{hfac})_3\text{NITet}$), they are expected to provide a paramagnetic contribution to the static susceptibility. We therefore devote this section to the detailed investigation of the magnetic properties in the $\text{Eu}(\text{hfac})_3\text{NITet}$ chain.

A. Magnetic susceptibility

The free ion Eu^{3+} presents a nonmagnetic 7F_0 ground state, with the excited levels 7F_1 and 7F_2 , respectively, at 504 and 1439 K. The magnetic susceptibility shown in Fig. 3 displays a maximum at about 12 K, followed by a decrease at low temperature. Even though this behavior might appear characteristic of quasi-1D systems, whereby the maximum corresponds to the development of short-range order due to antiferromagnetic coupling along the chain [24,25], it should be noted that the paramagnetic contribution of the free ion Eu^{3+} to the magnetic susceptibility cannot be neglected [26]. The model used to approximately describe the Eu chain therefore includes both an intrachain Hamiltonian and a free

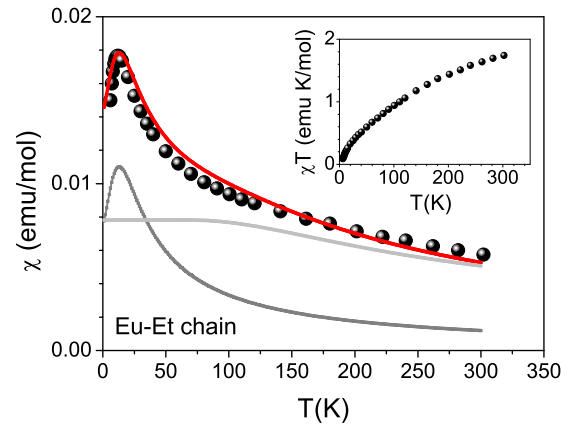


FIG. 3. The molar magnetic susceptibility (circles) of the $\text{Eu}(\text{hfac})_3\text{NITet}$ chain χ , measured versus temperature T , in an applied field of 0.1 T. The red line is a fit, obtained summing the theoretical expression (dark gray line) for a $s = 1/2$ Heisenberg antiferromagnetic chain [24,25] with intrachain exchange coupling constant $J = -20$ K between radical spins, and the free ion Eu^{3+} contribution (light gray line) calculated [26] in Appendix A. (Inset) The measured product χT (circles) versus T .

ion contribution,

$$\begin{aligned} \mathcal{H} &= \mathcal{H}_{\text{intra}} + \mathcal{H}_{\text{Eu}^{3+}} \\ &= -J \sum_{i=1}^{N-1} \mathbf{s}_i \cdot \mathbf{s}_{i+1} - g\mu_B \sum_{i=1}^N \mathbf{H} \cdot \mathbf{s}_i + \mathcal{H}_{\text{Eu}^{3+}}, \end{aligned} \quad (1)$$

where \mathbf{s}_i are the $s = 1/2$ radical spins localized on the N sites of a 1D lattice, $J < 0$ is the antiferromagnetic intrachain exchange coupling constant between radical spins, $g = 2$ the gyromagnetic factor, μ_B the Bohr magneton, and H the external magnetic field. The interchain coupling constant J_\perp was assumed to be negligible with respect to the intrachain one, J . The susceptibility could be adequately reproduced summing the theoretical expression by Bonner and Fisher [24,25] for the $s = 1/2$ Heisenberg antiferromagnetic chain, and the free ion Eu^{3+} contribution as reported by Lueken [26] (see also Appendix A). It is well known that the position and intensity of the peak are determined by the value of the intrachain exchange coupling. From Fig. 3 it appears that the best fit is obtained for $J = -20$ K. At temperatures lower than 100 K, the Eu^{3+} contribution is substantially constant and is given by the Larmor diamagnetism and the Van Vleck paramagnetism [27], while at higher temperatures its paramagnetic contribution decreases with increasing T , and becomes the main contribution for $T > 300$ K.

B. NMR linewidth and relaxation rates

The investigation of the static and dynamic properties of this compound was done through the analysis of the NMR proton absorption spectral width and the measurement of the proton nuclear spin-lattice relaxation rate (NSLR) $1/T_1$, as a function of temperature. These data have been collected in the temperature range $3 < T < 295$ K, with an applied static magnetic field $H \sim 0.33$ T that corresponds to the value $\nu = 14.1$ MHz of the Larmor frequency for protons (${}^1\text{H}$ nuclei).

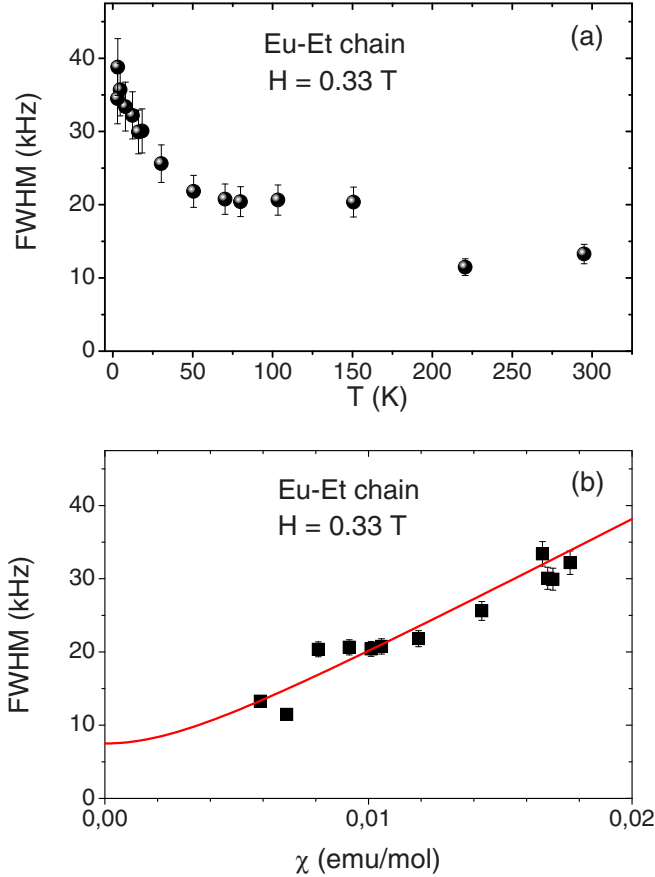


FIG. 4. (a) Full width at half maximum (FWHM) of the proton NMR line as a function of temperature in $\text{Eu}(\text{hfac})_3\text{NITet}$. (b) The measured inhomogeneous linewidth (full squares) plotted versus the magnetic susceptibility χ . The full line is a fit according to Eqs. (2) and (3).

The temperature behavior of the proton NMR linewidth as a function of temperature is shown in Fig. 4(a). Two contributions are responsible for the observed linewidth. The first one is a T - and H -independent term connected with the nuclear dipole-dipole interaction. The second term is related to the dipolar interaction of the protons with the thermal average of the magnetic moments of the radicals and of the Eu^{3+} free ion (excited levels). In the usual simple Gaussian approximation for the NMR line-shape, the linewidth is proportional to the square root of the second moment, which in turn is given by the sum of the second moments due to the two interactions [28,29],

$$\text{FWHM} \propto \sqrt{\langle \Delta v^2 \rangle_{\delta} + \langle \Delta v^2 \rangle_M}. \quad (2)$$

The second term represents the inhomogeneous broadening of the NMR line and is proportional to the average magnetization of the paramagnetic system,

$$\sqrt{\langle \Delta v^2 \rangle_M} = B_R \chi_R H + B_{\text{Eu}} \chi_{\text{Eu}} H, \quad (3)$$

where B_R is the dipolar interaction among the nuclei and the electrons of the radical groups, χ_R is the susceptibility of the $s = 1/2$ radical chain, B_{Eu} is the hyperfine interaction among the nuclei and the Eu^{3+} ion, and χ_{Eu} is the contribution to

the susceptibility of the Eu^{3+} free ion. Note that Eq. (3) is correct if the dipolar and hyperfine coupling tensors of both spins are diagonalized with the same principal axes. As in our system the principal axes of the dipolar (B_R) and hyperfine (B_{Eu}) tensors are almost the same, Eq. (3) applies.

From the plot in Fig. 4(b) it appears that Eqs. (2) and (3) do fit the experimental results with a nuclear dipolar second moment $\langle \Delta v^2 \rangle_{\delta} = 7.5^2 \text{ kHz}^2$, $B_R = 1075(33) \text{ (Hz mole)/(Gauss emu)}$, and $B_{\text{Eu}} = 651(33) \text{ (Hz mole)/(Gauss emu)}$, equivalent to hyperfine coupling constants $A_{z,R} = 15.1 \times 10^{22} \text{ cm}^{-3}$ and $A_{z,\text{Eu}} = 9.1 \times 10^{22} \text{ cm}^{-3}$, which are of the correct order of magnitude for the nuclear-electron dipolar interaction in molecular magnets [20]. To obtain the constants $A_{z,R}$ and $A_{z,\text{Eu}}$ from B_R and B_{Eu} , one observes that the resonance frequency in the local field can be expressed as (the subscripts “R” and “Eu” are omitted for clarity)

$$\nu_M = \frac{\gamma}{2\pi} A_z \langle \mu \rangle = \frac{\gamma}{2\pi} A_z \frac{M}{N_A} = \frac{\gamma}{2\pi} A_z \frac{\chi H}{N_A}, \quad (4)$$

where $\gamma/(2\pi) = 4257.6 \text{ Hz/Oe}$ is the proton gyromagnetic ratio, M is the molar magnetization, and N_A is Avogadro’s number. By equating this last expression to Eq. (3), one obtains the required conversion, i.e., $A_z = \frac{2\pi}{\gamma} N_A B \text{ cm}^{-3}$. The fact that the relation (3) is obeyed down to the lowest investigated temperature indicates that, for $T \geq 3 \text{ K}$, the system remains in the paramagnetic state.

The temperature dependence of the proton spin-lattice relaxation rate, $1/T_1$, is shown in Fig. 5(a). The T_1^{-1} results track the T dependence of $(\chi T)_R$, that is, the contribution (represented by the dark gray line in Fig. 3) of the $s = 1/2$ radicals chain to the total χT . This is demonstrated by the temperature independence of the quantity $[T_1(\chi T)_R]^{-1}$ which is plotted in Fig. 5(b).

The general expression for the nuclear spin-lattice relaxation rate, obtained from time-dependent perturbation theory in the weak collision approximation, is [20,28]

$$1/T_1 = \frac{1}{2} \gamma^2 \int \langle h_+(t) h_-(0) \rangle e^{i\omega_L t} dt, \quad (5)$$

where $\omega_L = \gamma H$ is the nuclear Larmor frequency. The quantities $h_{\pm}(t)$ are the time-dependent transverse (with respect to the applied field H) components of the hyperfine field, generated at the proton site by the magnetic moments of the radicals. For a dipolar interaction, the hyperfine field is simply proportional to s , the electronic spin moment. Thus, if the system is paramagnetic, one can assume the electronic spins as uncorrelated, and approximate the correlation function of the hyperfine field in Eq. (5) by a simple exponential function, decaying with a single correlation time $\tau = \omega_e^{-1}$. The expression (5) for the NSLR can then be rewritten as [20,21,30]

$$1/T_1 = A^2 \chi T \frac{\omega_e}{\omega_e^2 + \omega_L^2} \approx A^2 \chi T \frac{1}{\omega_e}, \quad (6)$$

where we have made the approximation $\omega_e \gg \omega_L$, and $\chi T \equiv (\chi T)_R$. In fact, in strongly coupled paramagnets (as the present case, see below), the electronic correlation frequency (ω_e) is much larger than the nuclear Larmor frequency (ω_L), for the magnetic field range used here. The constant A^2 in Eq. (6) is the average square of the fluctuating instantaneous nuclear-electron dipolar interaction, and is related to the hyperfine

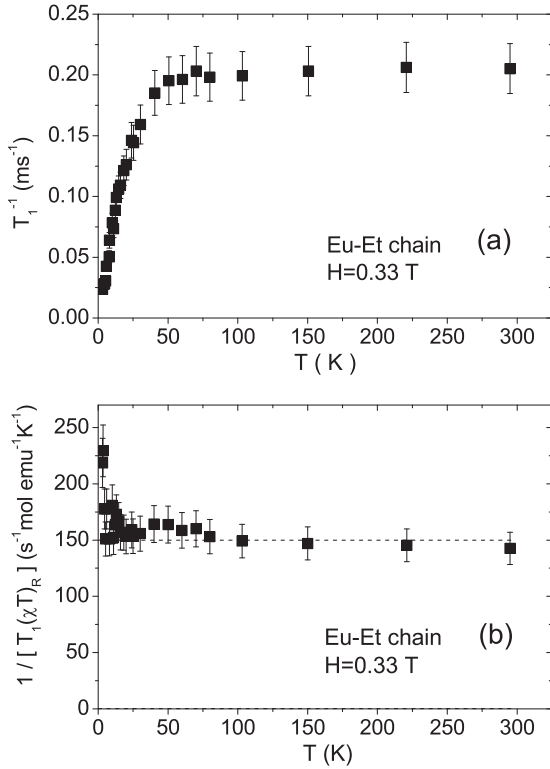


FIG. 5. (a) The proton spin-lattice relaxation rate $1/T_1$, of $\text{Eu}(\text{hfac})_3\text{NITet}$ at $H = 0.33$ T (resonance frequency $\nu = 14.1$ MHz) versus temperature T . (b) The same quantity, but reported in a plot which shows the temperature independence of $1/[T_1(\chi T)_R]$, although some scatter is present for $T < 75$ K. $(\chi T)_R$ represents the contribution of the $s = 1/2$ radicals chain to the total χT .

interaction constant A_z as shown further on. The fact that the quantity $(T_1 \chi T)^{-1}$ is T independent, as shown in Fig. 5(b), is a direct consequence of the T independence of the electronic correlation frequency ω_e in Eq. (6). According to Moriya's theory [30] of exchange coupled simple paramagnets, the exchange frequency is given by

$$\omega_e^2 = \frac{2z J^2 k_B^2}{3\hbar^2} [s(s+1)], \quad (7)$$

which yields $\omega_e = 2.6 \times 10^{12}$ rad/s, if one uses the value of the exchange constant $J = -20$ K, derived above from the magnetic susceptibility, and $z = 2$ as the number of nearest-neighbors of a given radical spin with $s = 1/2$. Then, from Eq. (6) one can estimate the value of the square root of the average square fluctuating nuclear-electron dipolar interaction (for radicals) to be $A \approx 2.2 \times 10^7$ rad/s. This corresponds to a hyperfine coupling constant $A_{z,R} = 9.1 \times 10^{22} \text{ cm}^{-3}$ (in order to convert the interaction constant A , measured in rad/s, into the hyperfine constant A_z , measured in cm^{-3} , one has to write A (rad/s) = $\gamma \mu_B A_z$, where γ is the gyromagnetic ratio for the proton and μ_B is the Bohr magneton, which is the instantaneous value of the fluctuating electronic moment for a spin $s = 1/2$). This value of the hyperfine constant $A_{z,R}$ is consistent with the one obtained above from the analysis of the FWHM versus the magnetic susceptibility, i.e., $A_{z,R} = 15.1 \times 10^{22} \text{ cm}^{-3}$, the difference being the result

of the different geometrical factors in the dipolar interaction tensor entering in the calculation of the NSLR and of the FWHM, respectively [28]. Since the geometrical factors in the dipolar interaction tensor scale as $1/r^3$, a hyperfine constant of $A_{z,R} = 10^{22} \div 10^{23} \text{ cm}^{-3}$ corresponds to distances between the proton and the local magnetic moment in the range $r = 2.2\text{--}4.7$ Å.

IV. RESULTS IN THE GADOLINIUM CHAIN

The substitution of diamagnetic Eu^{3+} by Gd^{3+} ions (with $S = 7/2$) changes completely the magnetic properties and the phase diagram of the material. From x-ray diffraction measurements [9], neighbor chains in $\text{Gd}(\text{hfac})_3\text{NITet}$ result in being well separated, as the minimum Gd-Gd distance is 10.5 Å. Hence one can conclude [4,10] that the ratio between interchain and intrachain exchange interactions is negligible ($\approx 10^{-4}$). The rich low temperature phenomenology of this compound arises from the competition between the intrachain nn FM interaction ($J_{z1} > 0$) and the nnn AFM exchange interactions ($J_{z2} < 0$, $J'_{z2} < 0$). The intrachain Hamiltonian of $\text{Gd}(\text{hfac})_3\text{NITet}$ can be written as [12]

$$\begin{aligned} \mathcal{H}_{\text{intra}} = & -J_{z1} \sum_{i=1}^{N/2} (\mathbf{S}_{2i-1} \cdot \mathbf{s}_{2i} + \mathbf{s}_{2i} \cdot \mathbf{S}_{2i+1}) \\ & - J_{z2} \sum_{i=1}^{N/2} \mathbf{S}_{2i-1} \cdot \mathbf{S}_{2i+1} - J'_{z2} \sum_{i=1}^{N/2} \mathbf{s}_{2i} \cdot \mathbf{s}_{2i+2} \\ & - g\mu_B \sum_{i=1}^{N/2} \mathbf{H} \cdot (\mathbf{S}_{2i-1} + \mathbf{s}_{2i}), \end{aligned} \quad (8)$$

where $J_{z1} = +5.05$ K is the Gd-radical exchange coupling, $J_{z2} = -0.98$ K is the Gd-Gd exchange coupling, and $J'_{z2} = -7.67$ K is the radical-radical exchange coupling [12]. The spins \mathbf{S}_{2i-1} and \mathbf{s}_{2i} of the Gd^{3+} ion and of the radical are, respectively, located on the odd and even sites of a 1D lattice, and are supposed to lie within a plane perpendicular to the chain axis; an external magnetic field H is possibly applied along a certain in-plane direction. A recent investigation [18], where low temperature specific heat, magnetic susceptibility, and zero-field muon spin resonance (μSR) measurements were performed jointly, suggested that $\text{Gd}(\text{hfac})_3\text{NITet}$ undergoes two distinct phase transitions, in agreement with a theoretical prediction known as the Villain's conjecture [23]. More precisely, a chiral spin liquid phase, where the spin chirality order parameter $\kappa_n = [\mathbf{S}_n \times \mathbf{S}_{n+1}]^z / |\sin(Qa)|$ is different from zero, sets in at the transition temperature $T_0 = 2.19$ K, followed by a 3D long-range helical phase, where the $SO(2)$ symmetry of the spin variable \mathbf{S}_i is spontaneously broken, which appears at the transition temperature $T_N = 1.88$ K (see Fig. 2). In the previous expression, Q is the modulus of the critical wave vector of the helical ground state, while \mathbf{S}_n and \mathbf{S}_{n+1} are spins on nearest-neighbor planes perpendicular to \mathbf{Q} . For $T = 0$ K, the order parameter $\kappa_n = \pm 1$ (similar to an Ising variable [31]) describes the clockwise or anticlockwise degeneracy Z_2 of the helical structure. In the usual 3D systems where chiral order and spin order occur simultaneously, the order parameter becomes $Z_2 \times SO(2)$, leading to a new universality class [32].

In the 1D regime, the Villain's conjecture instead predicts $T_0 > T_N$ because, as the temperature is decreased, the correlation length of the chirality (defined by $\langle \kappa_1 \kappa_{n+1} \rangle \sim e^{-na/\xi_\kappa}$) diverges exponentially, $\xi_\kappa \sim e^{J/T}$, while the correlation length for the spin variables (defined by $\langle \mathbf{S}_1 \cdot \mathbf{S}_{n+1} \rangle \sim e^{-na/\xi_S}$) diverges as a power law, $\xi_S \sim |J|/T$. As a consequence, it is clear that the spin chirality phase transition at temperature T_0 can be observed only through experimental results related to four-point correlation functions (like an anomaly in the specific heat), while experimental results related to two-point correlation functions (like magnetic susceptibility, muon spin resonance, NMR, etc.) present anomalies at the helical transition temperature T_N . In Ref. [18], two anomalies were observed in the specific heat for $T_0 = 2.19$ K and $T_N = 1.88$ K, while in the magnetic susceptibility and μ^+ SR data an anomaly was observed only for $T_N = 1.88$ K. The phase transitions in the Gd chain have recently been the subject of some debate [33], so it would be very interesting to probe directly the chirality, e.g., using polarized neutron scattering measurements [34,35]. Unfortunately, these experiments look unfeasible at the moment, since the crystals available so far are too small. In the absence of such a "smoking gun" for the chiral phase, the observations of Ref. [18] represent, to our knowledge, the best evidence for the realization of Villain's conjecture. The new proton NMR results presented in this work (see below) aim at confirming the above-described scenario, and obtaining new information about the critical spin dynamics in the vicinity of the helical phase transition.

A. Role of the external magnetic field

In the following, we report the experimental results obtained from magnetic susceptibility (more precisely M/H) and NMR measurements. Both of these techniques require the application of an external magnetic field H . It is, therefore, important to understand the effect of H at least on the magnetic ground state. When the field is applied in the easy plane, it is well known [36,37] that the magnetic behavior of the system can be complex depending on the intensity of H . For small H , there is only a slight distortion of the helix, with a small net magnetic moment along H . At such low fields, small effects on the magnetic susceptibility and NMR relaxation rate are expected. On the contrary, for very high fields, larger than a critical value H_P , all the spins will be aligned along the field direction, like in a paramagnetic system. For intermediate fields, a fan arrangement of the spins was hypothesized [36,38]. More precisely, the transition from the helical to the fan phase is expected to occur at a critical field value H_C , which usually is $\sim \frac{1}{2}H_P$. The transition is of first order at very low temperatures, and continuous near T_N [36,38]. Consequently, in order to understand the experimental results, it is very important to determine the value of H_P . Following Nagamiya *et al.* [39], this task can be simply accomplished. In Appendix A, we report the details of the calculation for H_P in the case of the Gd(hfac)₃NITet chain, where the presence of two different kinds of spins was explicitly taken into account [13]. We obtained $H_P = 6.56$ T, a value much higher than the field values exploited in the present investigation. In Appendix A, the distortion of the

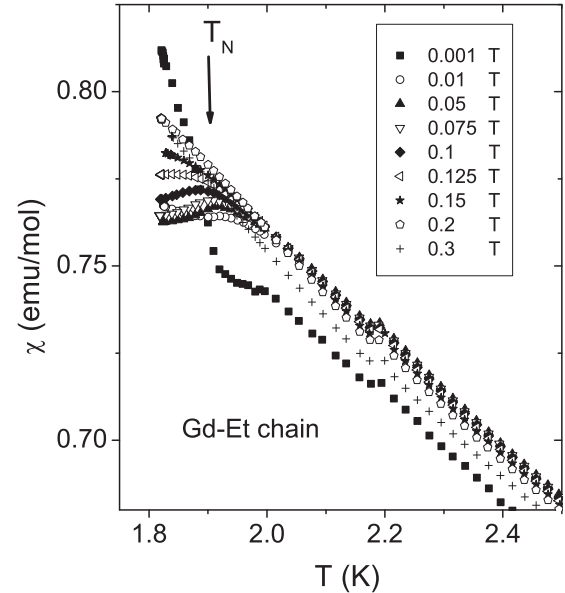


FIG. 6. Molar ratio M/H of Gd(hfac)₃NITet at different applied magnetic fields. Note that the measured quantity M/H for low fields approximately corresponds to the magnetic susceptibility χ . An anomaly at the transition temperature to 3D helical order, $T_N = 1.9$ K, is visible for $H \leq 0.125$ Tesla.

helical structure of Gd(hfac)₃NITet in the presence of a weak magnetic field is also calculated.

B. Magnetic measurements

The accepted theory [13,18], which explains most of the experimental data in the Gd-Et chain, predicts that the system is characterized by two critical magnetic fields: the first, $H_C \sim 3$ T, above which a fan spin structure is obtained and the second, $H_P = 6.56$ T, above which a collinear structure is realized [13]. On the other hand, the magnetic phase diagram in Fig. 2 and the subsequent magnetic behavior as a function of temperature are rigorously valid for $H = 0$. However, if a moderate magnetic field ($H \ll H_C$) is applied, one can infer that the magnetic response of the compound will remain essentially unaltered, because the field determines only a slight distortion of the helix with a small net moment along H . This can be seen in Fig. 6 where, for fields $H \leq 0.125$ T, an anomaly at $T_N = 1.9$ K, due to the phase transition to the 3D helical phase, can still be detected.

As the NMR measurements have to be performed in an applied magnetic field, we chose to investigate the nuclear relaxation and spectra at three magnetic fields, lower than H_C , compatible with the electronic limits in signal detection (i.e., $H = 0.1, 0.33$, and 1.4 T).

C. Proton NMR spectra

The ¹H NMR measurements were performed on a powder sample of Gd(hfac)₃NITet at three different static magnetic fields ($H = 0.1, 0.33$, and 1.4 T, corresponding to a resonance frequency of 4.25, 14.1, and 60 MHz, respectively) on ¹H nuclei in the temperature range $1.5 < T < 295$ K. At all the investigated frequencies, the spectra show a gradual line

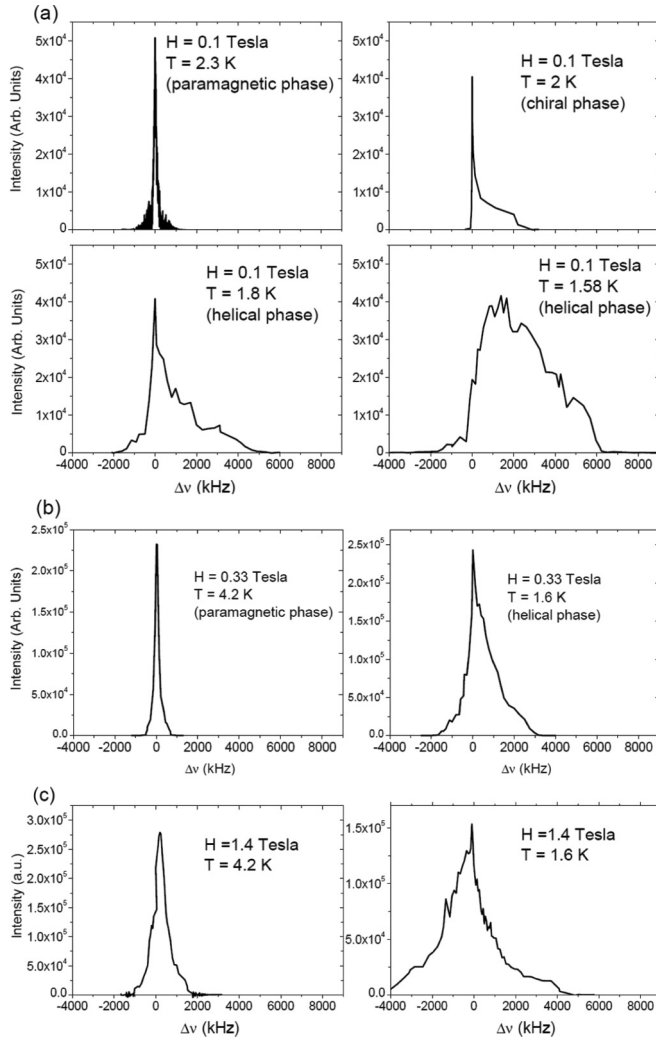


FIG. 7. Proton NMR spectra of $\text{Gd}(\text{hfac})_3\text{NITet}$ at (a) $H = 0.1$ T (resonance frequency $\nu = 4.25$ MHz); (b) $H = 0.33$ T (resonance frequency $\nu = 14.1$ MHz); (c) $H = 1.4$ T (resonance frequency $\nu = 60$ MHz). Taking into account that $T_N = 1.9$ K is the typical transition temperature to the 3D long-range helical order (see text), some representative temperatures are reported.

broadening on decreasing temperature, due to the increase of the paramagnetic magnetization, just like in the Eu chain [see Fig. 4(a) for comparison]. However, contrary to the Eu chain, the Gd chain, at the two lowest fields, displays a sudden, asymmetric, large inhomogeneous broadening of the NMR line below the transition temperature $T_N = 1.9$ K. On crossing the first transition at $T_0 = 2.2$ K, the broadening is only moderate, while on crossing the second transition at 1.9 K, the broadening is very severe. In fact, the measurements at $H = 0.1$ T (corresponding to the situation where the magnetic lattice is nearer to the situation of zero field) show that just above 2 K the FWHM is about 100 kHz, while at 1.9 K there is a sudden increase to 1 MHz and, at the lowest temperature measured, when the 3D transition is completed, the FWHM is ~ 3 MHz. These findings are illustrated in the representative spectra collected at different fields, shown in Fig. 7. As noted previously, the application of a small magnetic field, $H = 0.1$ T, should guarantee that the magnetic lattice of spins

is not distorted, while the situation is more complicated when $H = 0.33$ and 1.4 T are applied.

The inhomogeneous broadening is related to the freezing of the spins of the chains below the transition, with the consequent insurgence of a distribution of different local dipolar hyperfine fields at the proton sites, and thus a distribution of resonance frequencies. Contrary to the case of the paramagnetic phase (where the distribution of local fields generates a symmetric broadening, since the average paramagnetic moments are all aligned along the applied field), in the ordered spin fluid phase, $2.2 < T < 1.9$ K, and in the 3D long-range helical phase, $T < 1.9$ K, the distribution of resonance frequencies results in an asymmetric broadening, since the frozen spins have their own orientation independent of the applied field. It is noted that the asymmetric broadening is characteristic of the powder pattern observed in NMR, when there is a random distribution of orientations of the local field with respect to the external field [28]. An analysis and simulation of the NMR line profile could in principle provide important information on the magnetic spin structure in the chiral and helical phases if measurements could be performed in a single crystal [40]. Unfortunately, in the case of our compound, no single crystal large enough for NMR measurements could be grown. Some features of the asymmetric line profile expected for chiral and helical phases are retained even in the presence of a powder pattern (see Fig. 7), but the extraction of quantitative information about the magnetic spin structure becomes ambiguous. Thus we limit ourselves to a qualitative discussion of the NMR line profiles.

The broadening of the NMR line occurs mostly at the second phase transition, i.e., in the 3D helical phase. From Fig. 7 it is easy to observe that the broadening at the transition is more marked at the lowest field $H = 0.1$ T than at higher fields. This is consistent with the notion that an applied field tends to destroy the 3D long-range helical spin order (see Sec. IV A), giving rise to new more “disordered” spin structures. The effect of the external magnetic field on the magnetic and thermodynamic properties was seen also on the Gd-iPr analog, where the specific heat λ peak was found to broaden and disappear at high field [15].

D. Proton spin-lattice relaxation rate

In Fig. 8 we report some recovery curves for the nuclear longitudinal magnetization collected in a magnetic field $H = 0.1$ T (symbols) with the corresponding fitting function (solid lines). A multiexponential behavior was found, as in other molecular magnets [21], due to the existence of many inequivalent hydrogen sites. More precisely (as previously said in Sec. II) for the fit in Fig. 8 we used (in the temperature range $2 < T < 6$ K) the sum of two functions,

$$\frac{M_z(t) - M_z(0)}{M_z(0)} = A \exp[-(t/T_{1,\text{fast}})^\beta] + B \exp[-(t/T_{1,\text{slow}})^\beta], \quad (9)$$

namely the sum of (i) a fast-relaxing stretched exponential with $0.8 < \beta \leq 1$; (ii) a slow-relaxing stretched exponential with $\beta' = 0.5$ and a low percent weight (7%–19%) over the total magnetization. Please note that, due to the wipe-out effect, the

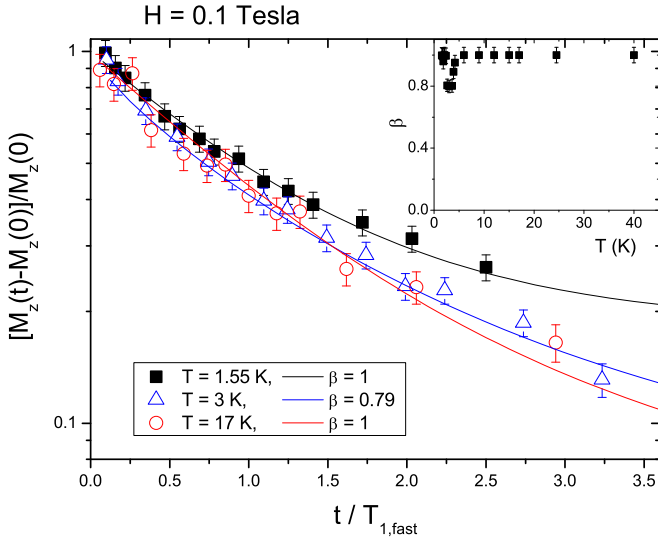


FIG. 8. Some typical relaxation curves of the nuclear longitudinal magnetization for $\text{Gd}(\text{hfac})_3\text{NITeT}$, at three different temperatures and $H = 0.1$ Tesla. The lines are fits to the experimental data (symbols) and they were obtained using a sum of two functions: $\frac{M_z(t) - M_z(0)}{M_z(0)} = A \exp[-(t/T_{1,\text{fast}})^\beta] + B \exp[-(t/T_{1,\text{slow}})^{\beta'}]$. The fast-relaxing function has a stretched exponential behavior with $0.8 < \beta \leq 1$; this component is the dominating one in the temperature range $2 < T < 6$ K. The slow-relaxing function is a stretched exponential with $\beta' = 0.5$; this component has a low percent weight over the total magnetization (7%–19%, depending on temperature and the wipe-out entity). The temperature behavior of $\beta(T)$ is reported in the inset.

slow-relaxing component slightly changes its relative weight with temperature.

In Fig. 9(a), we report the temperature dependence of the longitudinal relaxation rate T_1^{-1} , collected at constant applied field $H = 1.4$ T (corresponding to $\nu = 60$ MHz), $H = 0.33$ T ($\nu = 14.1$ MHz), and $H = 0.1$ T ($\nu = 4.25$ MHz). The data for T_1^{-1} were obtained from the fast-relaxing function, which pertains to hydrogen nuclei in the proximity of magnetic ions. It is noted that the slow-relaxing function is attributed to hydrogen nuclei very weakly coupled to the magnetic ions, and does not reflect the electron spin dynamics.

The behavior of $1/T_1(T)$ is different for the lowest fields ($H = 0.1$ T and $H = 0.33$ T) and the highest one ($H = 1.4$ T). At $H = 0.1$ T and $H = 0.33$ T, $1/T_1(T)$ displays the weak temperature dependence typical of paramagnetic spin dynamics down to temperatures as low as 4 K, similarly to the case of the Eu chain and, on approaching the phase transition temperatures $T_0 = 2.2$ K and $T_N = 1.9$ K, it undergoes a critical enhancement, reaching a peak at 1.9 K, where an extraordinary loss of signal (see discussion later on) is also observed. At $H = 1.4$ T, the nuclear longitudinal relaxation rate shows again an enhancement for $T < 4$ K, but now the peak is at higher temperature, namely $T \sim 3$ K.

Let us now focus on the $1/T_1$ versus T data at $H = 0.1$ T, i.e., the situation for which one has a nondistorted spin lattice. First, it should be reminded that, for a magnetic system undergoing a phase transition to an ordered phase, both the NSLR ($1/T_1$) and the homogeneous part of the NMR linewidth ($1/T_2$) are expected to diverge on approaching the

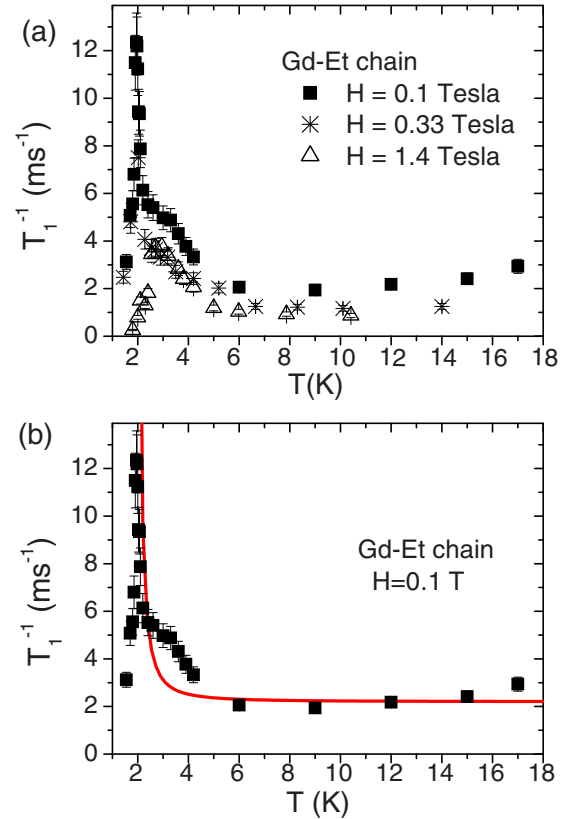


FIG. 9. The nuclear spin-lattice relaxation rate, measured at (a) three different magnetic fields and (b) $H = 0.1$ T ($\nu = 4.25$ MHz, full squares), compared with the divergent behavior predicted by Eq. (10) (full line). Around $T = 1.9$ K, the data were collected with a resolution of 0.02 K.

critical temperature T_N . The enhancement is associated with the divergent behavior of the response function in Eq. (5), and the corresponding slowing down of the electronic spin fluctuations represented by the decrease (on diminishing T) of the correlation frequency ω_e in Eq. (6). By combining the two effects, and exploiting the fluctuation-dissipation theorem and the dynamical scaling approximation [41,42], one predicts a critical behavior of the form [15,21],

$$\begin{aligned} 1/T_1 \approx 1/T_2 \propto \frac{1}{\omega_e} \xi^{z-d+2-\eta} \propto (T - T_N)^{-\nu(z-d+2-\eta)} \\ \propto (T - T_N)^{-5/3}. \end{aligned} \quad (10)$$

In Eq. (10) we assumed a correlation length which diverges as $\xi \propto (T - T_N)^{-\nu}$ and a space dimensionality $d = 1$. Regarding the dynamical critical exponents, we assumed the ones pertaining to the $SO(2)$ universality class, valid for helical antiferromagnets [41,42], namely $z = 1.5$, $\nu = 2/3$, $\eta = 0$. However, it is worth observing that our experimental data do not allow discerning between different universality classes, although they unequivocally signal a critical behavior.

The result in Eq. (10) predicts a divergent behavior of both the longitudinal ($1/T_1$) and the transverse ($1/T_2$) relaxation rates, on approaching the transition temperature from the high temperature side. The low temperature data for $1/T_1$ versus

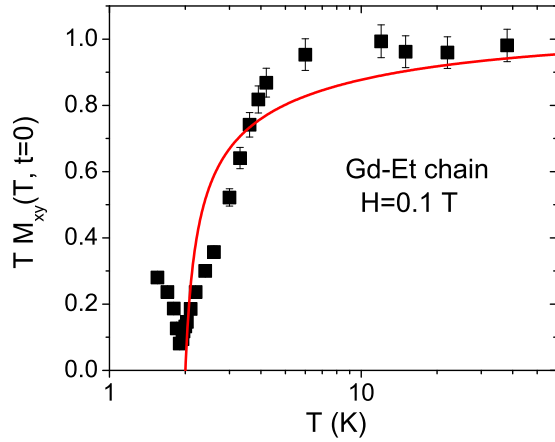


FIG. 10. The normalized proton NMR signal loss (full squares) of $\text{Gd}(\text{hfac})_3\text{NITeEt}$, $T \times M_{xy}(T, t=0)$, versus temperature T , compared with the theoretical curve Eq. (11) (full line), calculated with $T_N = 1.9$ K and $C = 0.35$ K $^{2/3}$.

temperature at the lowest field $H = 0.1$ T (corresponding to the situation of the less perturbed electron spin system) are plotted in Fig. 9(b) (full squares) and compared with the enhancement predicted by Eq. (10) (solid line). The divergent behavior in the NSLR is clearly visible, although a precise value of the critical exponent cannot be obtained owing to the limited number of experimental points in the critical region. Thus the comparison between theory and experiment can only be qualitative and the critical exponent in Eq. (10) has to be viewed only as indicative. This is due to the fact that the divergent behavior, occurring in the transverse relaxation rate at the same temperature as the one occurring in the longitudinal relaxation rate, produces a sudden (i.e., in a very small temperature range, of the order of $\Delta T \sim 0.04$ K) homogeneous broadening of the NMR line which generates a wipe-out effect, with subsequent signal loss. In fact, the homogeneous broadening corresponds to an irreversible decay of the nuclear magnetization that cannot be refocused with the Hahn echo method. Thus, since the echo signal decays very fast, it falls within the “blind electronics (response) time” of the NMR spectrometer, and a sudden decrease of the signal intensity is observed. The wipe-out effect has been analyzed in other cases, and a simple model has been adopted to describe it [43]. According to this model, the fraction of nuclei which are detected, $n(T)/n_0$, is related to the correlation time τ of the hyperfine field fluctuations by the expression [43],

$$\begin{aligned} n(T)/n_0 &= 1 - C'\tau^{0.5} = 1 - C\epsilon^{-0.5z\nu} \\ &= 1 - C\epsilon^{-1/2} = 1 - C(T - T_N)^{-1/2}, \quad (11) \end{aligned}$$

where we have assumed [22,42] for the critical correlation frequency a critical behavior $\tau^{-1} \approx k^z$, with the inverse two-spin correlation length given by $k = k_0\epsilon^\nu$, and the same critical exponents as in Eq. (10). The constant $C = 0.35$ K $^{2/3}$ in Eq. (11) incorporates several parameters related to the strength of the fluctuating hyperfine field and to the “blind electronics (response) time” of the spectrometer. However, its absolute value, which is adjusted as a fitting parameter, is irrelevant for the discussion of the data. In Fig. 10 we compare the

experimental wipe-out of the proton NMR signal at $H = 0.1$ T [which can be plotted as the transverse nuclear magnetization at time $t = 0$, i.e., $M_{xy}(T, t = 0)$, times the temperature T] versus temperature (square symbols), with the prediction of Eq. (11) (solid line). It is noted that the wipe-out effect occurring at T_N is indeed a critical effect, indicating the critical enhancement and slowing down of spin fluctuations at the 3D magnetic phase transition.

Below the transition temperature, the electronic spins become frozen at the time scale of the NMR experiment (\approx MHz). As a consequence, the homogeneous broadening (i.e., $1/T_2$) recovers its normal value, determined by the nuclear dipolar interaction, and the NMR signal can be again refocused by the spin echo technique, as shown by the rise of the quantity $M_{xy}(T, t = 0) \times T$ at low temperature (see Fig. 10). However, it should be noted that, in the ordered magnetic state below $T_N = 1.9$ K, the NMR signal becomes inhomogeneously broadened by the distribution of static local fields. Thus the detected NMR signal remains small, since it arises only from the portion of the total spectrum covered by the radio frequency (rf) bandwidth of the excitation rf pulse.

E. Discussion and conclusions

In conclusion, the $\text{RE}(\text{hfac})_3\text{NITeEt}$ (RE=Eu, Gd) molecular magnetic chains were investigated using the NMR technique with the aim of highlighting the local spin dynamics. The Europium-based system displayed a paramagnetic behavior down to very low temperature ($T \approx 3$ K), without any phase transition to a magnetic ordered state. This is demonstrated by the FWHM versus temperature collected at $\nu = 14.1$ MHz, which shows no sudden line broadening, and by the spin-lattice relaxation rate, which is simply proportional to the magnetic susceptibility obtained for a 1D $s = 1/2$ AF chain with a temperature-independent spin-spin correlation frequency of the order of 10^{12} Hz. The intrachain exchange coupling constant between the radical centers was determined to be $J = -20$ K from the fit of susceptibility measurements. It should be noted that the 3D transition to an ordered phase at very low temperature would have to be triggered by the weak interchain interaction J_\perp . In a simple mean field approximation, one can estimate [44] the 3D transition temperature to be $T_C \approx 2\sqrt{JJ_\perp}(s+1)$, where J is the intrachain exchange interaction. For the Eu-Et chain, assuming $s = 1/2$, $J = -20$ K, and $J_\perp/J \approx 10^{-4}$, one has $T_N \approx 0.3$ K, which is consistent with the fact that the system behaves as a 1D paramagnet down to the lowest investigated temperature (i.e., $T = 3$ K). The Gadolinium-based compound displayed the two-step magnetic ordering sequence first predicted by Villain [23] and later confirmed by joint specific heat, susceptibility, and μSR measurements [18]. In our NMR experiment, the onset of the ordered chiral phase at $T_0 = 2.2$ K is detected only by the small asymmetric broadening of the proton NMR line, due to the partial freezing of the moments (see Fig. 7). No critical effects on the spin dynamics can be detected at T_0 , since NMR is sensitive only to the two-spin correlation function, which is noncritical at the chiral phase transition [14,18]. On the other hand, the 3D long-range helical phase, setting in at $T_N = 1.9$ K, was detected by a

sudden increase in the linewidth of the proton NMR spectra (see Fig. 7), a narrow peak in the nuclear longitudinal relaxation rate $1/T_1$ (see Fig. 8), and a loss of the NMR signal due to the critical divergence of the transverse relaxation rate (see Fig. 10). It should be remarked that the relatively high 3D transition temperature, i.e., $T_N = 1.9$ K in the Gd-Et chain, compared to the Eu-Et chain which remains paramagnetic down to very low temperature, must be due partly to the large Gd spin, $S = 7/2$, and partly to the much faster divergence of the chiral correlation length [14,18] as temperature is decreased, while the ratio between the interchain and the intrachain magnetic couplings is similar in both compounds ($J_{\perp}/J \approx 10^{-4}$). Finally it is noted that the NMR technique, which uses a local probe, resulted to be very sensitive, since a phase transition was detected both at $H = 0.1$ T and $H = 0.33$ T. In contrast, exploiting other macroscopic techniques, such as susceptibility and specific heat, the anomalies signaling the phase transition were found to be smooth, and disappeared already at $H = 0.1$ T [18]. In conclusion, the detailed evolution of the magnetic phase in the Gd-Et chain at magnetic fields of the order of (or higher than) 0.1 T could be pursued by NMR measurements, and related theoretical analysis, so as to obtain the complete phase diagram of this interesting system.

where

$$\mu_{\text{eff}}^2 = Z^{-1} \left\{ 144 \frac{k_B T}{\zeta} + \left(\frac{27}{2} - 9 \frac{k_B T}{\zeta} \right) e^{-\frac{\zeta}{6k_B T}} + \left(\frac{135}{2} - 15 \frac{k_B T}{\zeta} \right) e^{-\frac{\zeta}{2k_B T}} + \left(189 - 21 \frac{k_B T}{\zeta} \right) e^{-\frac{\zeta}{k_B T}} + \left(405 - 27 \frac{k_B T}{\zeta} \right) e^{-\frac{5\zeta}{3k_B T}} + \left(\frac{1485}{2} - 33 \frac{k_B T}{\zeta} \right) e^{-\frac{5\zeta}{2k_B T}} + \left(\frac{2457}{2} - 39 \frac{k_B T}{\zeta} \right) e^{-\frac{7\zeta}{2k_B T}} \right\}, \quad (\text{A3})$$

and

$$Z = \{ 1 + 3e^{-\frac{\zeta}{6k_B T}} + 5e^{-\frac{\zeta}{2k_B T}} + 7e^{-\frac{\zeta}{k_B T}} + 9e^{-\frac{5\zeta}{3k_B T}} + 11e^{-\frac{5\zeta}{2k_B T}} + 13e^{-\frac{7\zeta}{2k_B T}} \}. \quad (\text{A4})$$

We note that ζ , which is related to the spin-orbit coupling parameter λ_{LS} by $\zeta = 6\lambda_{\text{LS}}$ [26], was assumed as a free parameter in order to take into account also the contribution of the ligand field. The best fit reported in Fig. 3 was obtained using $\zeta = 2302$ K. Finally, the contribution of the ground state 7F_0 of the free ion Eu^{3+} to the Larmor diamagnetic susceptibility was fitted, $\chi_m^{\text{dia}} = -0.001$, in order to obtain the correct value of magnetic susceptibility at $T = 300$ K.

APPENDIX B: EFFECT OF AN EXTERNAL MAGNETIC FIELD ON THE GROUND STATE

We start from the intrachain Hamiltonian of $\text{Gd}(\text{hfac})_3\text{NITeT}$ (8) where [12] $\mu = g_{\text{Gd}}\mu_B = g_{\text{R}}\mu_B$ with $g_{\text{Gd}} = g_{\text{R}} = 2$. In the following we assume classical spins which in the ground state lie in the xy plane, perpendicular to the chain axis z . For this to happen, it is sufficient that the spins of Gd^{3+} ions are subjected to an easy-plane anisotropy. For zero applied field, the classical helical ground state is, therefore, characterized by polar angle $\theta_n = \frac{\pi}{2} \forall n$ (where θ_n is the angle formed by the n th classical spin vector with the z

ACKNOWLEDGMENTS

The Italian FIRB Project ‘‘Futuro in Ricerca’’ Grant No. RBFR12RPD1 and the EU Project MAGMANET Contract No. NMP3-CT-2005-515767 are acknowledged for funding.

APPENDIX A: CONTRIBUTIONS TO THE MOLAR MAGNETIC SUSCEPTIBILITY

For the sake of completeness, in this appendix we report (in cgs units) the various expressions exploited for the fit of magnetic susceptibility data reported in Fig. 3.

The molar magnetic susceptibility of a 1D $s = 1/2$ Heisenberg chain with antiferromagnetic exchange constant $J < 0$ can be expressed as [24,25]

$$\chi_m^{1D} = \frac{N_A \mu_B^2}{k_B T} \frac{g^2(0.25 + 0.0750x + 0.0752x^2)}{1 + 0.9931x + 0.1721x^2 + 0.7578x^3}, \quad (\text{A1})$$

where N_A is Avogadro’s number, μ_B Bohr’s magneton, k_B Boltzmann’s constant, $g = 2$ the gyromagnetic factor, and $x = |J|/(k_B T)$.

The paramagnetic contribution to the molar magnetic susceptibility of the free ion Eu^{3+} is expressed as [26]

$$\chi_m^{\text{para}} = \frac{N_A \mu_B^2}{3k_B T} \mu_{\text{eff}}^2, \quad (\text{A2})$$

axis), and critical wave vector of modulus Q given by

$$\pm Qa = \pm \cos^{-1} \left[-\frac{1}{2} \frac{sS J_{z1}}{J_{z2} S^2 + J'_{z2} S^2} \right], \quad (\text{B1})$$

where \pm denote the two possible chiralities of the helix. In the following, for the sake of simplicity, we will assume the external magnetic field to be applied along the x axis in the plane perpendicular to the chain axis: $\mathbf{H} = H\mathbf{x}$. Denoting by ϕ_n the angle formed by the n th classical spin vector with the x axis, the ground-state energy is obtained minimizing the expression,

$$E_0 = \sum_{n=1}^{N/2} \left\{ -\mu H [S \cos \phi_{2n+1} + s \cos \phi_{2n}] - J_{z1} s S [\cos(\phi_{2n+1} - \phi_{2n}) + \cos(\phi_{2n-1} - \phi_{2n})] - \frac{J_{z2}}{2} S^2 [\cos(\phi_{2n+1+2} - \phi_{2n+1}) + \cos(\phi_{2n+1-2} - \phi_{2n+1})] - \frac{J'_{z2}}{2} S^2 [\cos(\phi_{2n+2} - \phi_{2n}) + \cos(\phi_{2n-2} - \phi_{2n})] \right\}, \quad (\text{B2})$$

with respect to ϕ_{2n} and ϕ_{2n+1} (i.e., the azimuthal angles on the even and odd sites, respectively). The stationary conditions are

$$\begin{aligned} \frac{\partial E_0}{\partial \phi_{2n}} &= J_{z1} s S [\sin(\phi_{2n} - \phi_{2n-1}) - \sin(\phi_{2n+1} - \phi_{2n})] \\ &+ \frac{J'_{z2}}{2} s^2 [\sin(\phi_{2n} - \phi_{2n-2}) - \sin(\phi_{2n+2} - \phi_{2n})] \\ &+ \mu H s \sin \phi_{2n} = 0, \end{aligned} \quad (\text{B3})$$

$$\begin{aligned} \frac{\partial E_0}{\partial \phi_{2n+1}} &= J_{z1} s S [\sin(\phi_{2n+1} - \phi_{2n}) - \sin(\phi_{2n+2} - \phi_{2n+1})] \\ &+ \frac{J_{z2}}{2} S^2 [\sin(\phi_{2n+1} - \phi_{2n-1}) - \sin(\phi_{2n+3} - \phi_{2n+1})] \\ &+ \mu H S \sin \phi_{2n+1} = 0. \end{aligned} \quad (\text{B4})$$

For $H = 0$, one readily finds that in the ground state $\phi_n = nQa$, $\forall n$. Hereafter, the effect of a nonzero H on the ground-state energy E_0 will be considered in two limiting cases: weak and strong magnetic field.

A. Weak magnetic field

When a weak magnetic field is applied along the x axis (in the xy plane perpendicular to the chain axis), Eqs. (B3) and (B4) can be solved in a perturbative way following Nagamiya and coworkers [36,39], i.e., letting

$$\phi_n = nQa + \delta\phi_n, \quad (\text{B5})$$

where the small angular deviation $\delta\phi_n$ is proportional to the field. In the present case, characterized by two different kinds of spins on the odd and even sites of the chain and two different values of the next-nearest-neighbor exchange coupling, we will have different solutions of Eqs. (B3) and (B4) for even and odd sites,

$$\phi_{2n} = (2n)Qa + A_{\text{even}} \sin(2nQa), \quad (\text{B6})$$

$$\phi_{2n+1} = (2n+1)Qa + A_{\text{odd}} \sin[(2n+1)Qa], \quad (\text{B7})$$

where

$$\begin{aligned} A_{\text{even}} &= -\frac{\mu H}{D} 2s S J_{z1} \left\{ \cos(Qa) [S + s \cos(Qa)] \right. \\ &\left. + \delta_G \frac{S}{2} \cos(2Qa) [1 - \cos(2Qa)] \right\}, \end{aligned} \quad (\text{B8})$$

$$\begin{aligned} A_{\text{odd}} &= -\frac{\mu H}{D} 2s S J_{z1} \left\{ \cos(Qa) [s + S \cos(Qa)] \right. \\ &\left. + \delta_R \frac{S}{2} \cos(2Qa) [1 - \cos(2Qa)] \right\}. \end{aligned} \quad (\text{B9})$$

In the previous equations we have put

$$\delta_G = \frac{J_{z2} S}{J_{z1} S}, \quad \delta_R = \frac{J'_{z2} S}{J_{z1} S}, \quad (\text{B10})$$

and

$$\begin{aligned} D &= -4s^2 S^2 J_{z1} \cos^4(Qa) \\ &+ \{2s S J_{z1} \cos(Qa) + J'_{z2} \cos(2Qa) [1 - \cos(2Qa)]\} \\ &\times \{2s S J_{z1} \cos(Qa) + J_{z2} \cos(2Qa) [1 - \cos(2Qa)]\}. \end{aligned} \quad (\text{B11})$$

From these equations it appears that, for small H , there is only a slight distortion of the helix, with a small net magnetic moment along H . Consequently, very small effects on the magnetic susceptibility and NMR relaxation rate are expected.

In the case of equal spins ($s = S$) and equal next-nearest-neighbor exchange couplings ($J'_{z2} = J_{z2} = J_2$), one clearly obtains $A_{\text{even}} = A_{\text{odd}} = A$, with

$$\begin{aligned} A &= [-\mu H \sin(Qa)] \{2J_1 S \cos(Qa) [1 - \cos(Qa)] \\ &+ 2J_2 S \cos(2Qa) [1 - \cos(2Qa)]\}^{-1}. \end{aligned} \quad (\text{B12})$$

B. Strong magnetic field: determination of the critical field H_P

Even in the presence of a strong magnetic field, we will generalize a theory first developed by Nagamiya *et al.* [36,39], in order to treat the present case of two different kinds of spins, and two different values of the next-nearest-neighbor exchange coupling. For the sake of simplicity, the case of a single crystal sample will be considered hereafter. The application of a very strong field tends to align all the spins along the field direction. As before, we define ϕ_n as the angle between the n th spin and the field H . In a strong field, the deviations will be very small and different for the two kinds of spins. We then introduce the new variables,

$$x_{2n} = \sin\left(\frac{\phi_{2n}}{2}\right), \quad y_{2n+1} = \sin\left(\frac{\phi_{2n+1}}{2}\right), \quad (\text{B13})$$

where we assume $x_{2n} \ll 1$ and $y_{2n+1} \ll 1$. Next, expanding the energy (B2) in terms of x_{2n} and y_{2n+1} , considering only second-order contributions, and introducing the Fourier transforms

$$x_{2n} = \sum_{q \in BZ} \xi_q e^{i2nqa}, \quad y_{2n+1} = \sum_{q \in BZ} \eta_q e^{i(2n+1)qa}, \quad (\text{B14})$$

we obtain

$$\frac{E_0}{N} = c_0 + \epsilon_0^{(2)}, \quad (\text{B15})$$

where

$$c_0 = -J_{z1} s S - \left(\frac{J_{z2}}{2} S^2 + \frac{J'_{z2}}{2} s^2 \right) - \frac{\mu H}{2} (s + S), \quad (\text{B16})$$

$$\epsilon_0^{(2)} = \sum_{q \in BZ} [a_{11} |\xi_q|^2 + a_{12} (\eta_q \xi_q^* + \xi_q^* \eta_q) + a_{22} |\eta_q|^2], \quad (\text{B17})$$

and

$$a_{11} = 2J'_{z2} S^2 [1 - \cos(qa)] + 2J_{z1} s S + \mu H s, \quad (\text{B18})$$

$$a_{22} = 2J_{z2} S^2 [1 - \cos(qa)] + 2J_{z1} s S + \mu H S, \quad (\text{B19})$$

$$a_{12} = a_{21} = -2J_{z1} s S \cos(Qa). \quad (\text{B20})$$

The quadratic form $\epsilon_0^{(2)}$ can be diagonalized using new variables $\tilde{\xi}_q$ and $\tilde{\eta}_q$,

$$\epsilon_0^{(2)} = \sum_{q \in BZ} [\alpha_-(q, H) |\tilde{\xi}_q|^2 + \alpha_+(q, H) |\tilde{\eta}_q|^2], \quad (\text{B21})$$

and the eigenvalues are

$$\alpha_{\pm}(q) = \frac{a_{11} + a_{22}}{2} \pm \sqrt{(a_{11} - a_{22})^2 + 4a_{12}^2}. \quad (\text{B22})$$

From (B21) one observes that, if both the eigenvalues α_{\pm} are positive $\forall q$, the minimum of $\epsilon_0^{(2)}$ is obtained for $|\tilde{\xi}_q| = |\tilde{\eta}_q| = 0 \forall q$. This implies that $x_{2n} = y_{2n+1} = 0$, meaning [see Eq. (B13)] that all the spins are aligned with the field H . The critical field H_P , above which the ground state becomes collinear ferromagnetic can now be estimated taking into account that $\alpha_+(q, H) \geq \alpha_-(q, H)$, and imposing

$$\alpha_-(q, H) \geq 0 \quad \forall q. \quad (\text{B23})$$

The previous condition is satisfied for $H \geq \tilde{H}_P(q)$, where $\tilde{H}_P(q)$ is given by

$$\begin{aligned} \mu \tilde{H}_P(q) = & -\{[1 - \cos(2qa)](SJ_{z2} + sJ'_{z2}) + (s + S)J_{z1}\} \\ & + \{[1 - \cos(2qa)](SJ_{z2} - sJ'_{z2}) + (s - S)J_{z1}\}^2 \\ & + 4sSJ_{z1}^2 \cos^2(qa)\}^{1/2}. \end{aligned} \quad (\text{B24})$$

Finally, one can define the critical field as

$$H_P \equiv \max_{q \in BZ} \tilde{H}_P(q). \quad (\text{B25})$$

In the special case $S = s$ and $J_{z2} = J'_{z2}$, one readily observes that the maximum of $\tilde{H}_P(q)$ is obtained for $q = Q$, where Q is the modulus of the critical wave vector of the helical ground state [36,39] in $H = 0$. In the more general case under study, the position of the maximum and Q do not coincide, as shown in Fig. 11, where we plot the function $\tilde{H}_P(q)$ in the case of Gd(hfac)₃NITeT. The maximum is obtained for $q = \pi/(2a)$, namely for a value substantially different from

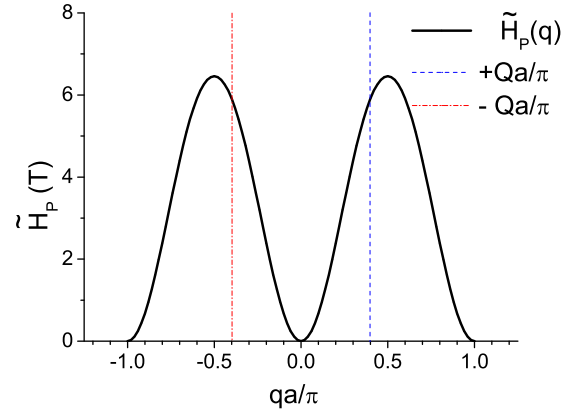


FIG. 11. Plot of the function $\tilde{H}_P(q)$, defined in Eq. (B24), in the case of Gd(hfac)₃NITeT. The maximum is obtained for $qa/\pi = 0.5$, to be compared with $Qa/\pi = 0.397$, the modulus of the critical wave vector of the helical ground state [12] for $H = 0$. The value of the critical field, defined in Eq. (B25), is $H_P = 6.46$ T.

$Q = 0.397\pi/a$, the modulus of the critical wave vector of the helical ground state [12] for $H = 0$. Substituting $q = \pi/(2a)$ in the expression (B24) for $\tilde{H}_P(q)$, from the definition (B25) we obtain the value $H_P = 6.46$ T for the critical field of Gd(hfac)₃NITeT. This is a huge field, much greater than the ones used in the experiments reported in the present work.

As regards the other critical field H_C , above which the transition to the fan phase takes place, its determination is not yet available in the case of a model with two kinds of spins and two different values of the next-nearest-neighbor exchange coupling. However, in the simpler case of rare-earth compounds where $S = s$ and $J_{z2} = J'_{z2}$, it was estimated [37] that $H_C \approx H_P/2$. For Gd(hfac)₃NITeT, this leads to $H_C \approx 3$ T, implying that some modification to the helical ground state might occur at the highest field ($H = 1.4$ T) used in our experiments while, for the two lower magnetic fields ($H = 0.1$ and 0.33 T), the modification should not be relevant.

-
- [1] E. Coronado, M. Drillon, A. Fuentes, D. Beltran, A. Mosset, and J. Galy, *J. Am. Chem. Soc.* **108**, 900 (1986).
- [2] M. Drillon, E. Coronado, D. Beltran, J. Curely, R. Georges, P. R. Nugteren, L. J. de Jongh, and L. J. Genicon, *J. Magn. Magn. Mater.* **54–57**, 1507 (1986).
- [3] J. S. Miller, J. C. Calabrese, A. J. Epstein, R. W. Bigelow, J. H. Zhang, and W. M. Reiff, *J. Chem. Soc., Chem. Commun.* 1026 (1986).
- [4] A. Caneschi *et al.*, *J. Am. Chem. Soc.* **109**, 2191 (1987); *Inorg. Chem.* **27**, 1756 (1988); **28**, 2940 (1989); *Angew. Chem. Int. Ed.* **40**, 1760 (2001); *Europhys. Lett.* **58**, 771 (2002).
- [5] A. Lascialfari *et al.*, *J. Appl. Phys.* **93**, 8749 (2003).
- [6] E. Micotti *et al.*, *J. Magn. Magn. Mater.* **272–276**, 1087 (2004).
- [7] M. Mariani *et al.*, *Inorg. Chim. Acta* **360**, 3903 (2007).
- [8] C. Benelli *et al.*, *J. Phys. (Paris) Colloq.* **49**, C8-861 (1988); *Inorg. Chem.* **28**, 3230 (1989); *J. Magn. Magn. Mater.* **140–144**, 1649 (1995).
- [9] C. Benelli *et al.*, *Inorg. Chem.* **28**, 275 (1989).
- [10] C. Benelli *et al.*, *Inorg. Chem.* **29**, 4223 (1990); *J. Appl. Phys.* **73**, 5333 (1993).
- [11] L. Bogani, C. Sangregorio, R. Sessoli, and D. Gatteschi, *Angew. Chem. Int. Ed.* **44**, 5817 (2005).
- [12] F. Bartolomé, J. Bartolomé, C. Benelli, A. Caneschi, D. Gatteschi, C. Paulsen, M. G. Pini, A. Rettori, R. Sessoli, and Y. Volokitin, *Phys. Rev. Lett.* **77**, 382 (1996).
- [13] C. Cucci, Master thesis in physics, Università degli Studi di Firenze, 1996.
- [14] M. Affronte, A. Caneschi, C. Cucci, D. Gatteschi, J. C. Lasjaunias, C. Paulsen, M. G. Pini, A. Rettori, and R. Sessoli, *Phys. Rev. B* **59**, 6282 (1999).
- [15] A. Lascialfari, R. Ullu, M. Affronte, F. Cinti, A. Caneschi, D. Gatteschi, D. Rovai, M. G. Pini, and A. Rettori, *Phys. Rev. B* **67**, 224408 (2003).
- [16] F. Cinti *et al.*, *Polyhedron* **24**, 2568 (2005).
- [17] F. Cinti *et al.*, *J. Magn. Magn. Mater.* **310**, 1460 (2007).

- [18] F. Cinti, A. Rettori, M. G. Pini, M. Mariani, E. Micotti, A. Lascialfari, N. Papinutto, A. Amato, A. Caneschi, D. Gatteschi, and M. Affronte, *Phys. Rev. Lett.* **100**, 057203 (2008).
- [19] C. Benelli, A. Caneschi, D. Gatteschi, J. Laugier, and P. Rey, *Angew. Chem. Int. Ed. Engl.* **26**, 913 (1987).
- [20] F. Borsa, A. Lascialfari, and Y. Furukawa, in *Novel NMR and EPR Techniques*, edited by J. Dolinsek, M. Vilfan, and S. Zumer (Springer-Verlag, Berlin, 2006), p. 297.
- [21] F. Borsa and A. Rigamonti, in *Magnetic Resonance at Phase Transitions*, edited by F. J. Owens, C. P. Poole, and H. A. Farach (Academic Press, New York, 1979), p. 79.
- [22] C. Benelli, A. Caneschi, D. Gatteschi, L. Pardi, P. Rey, D. P. Shum, and R. L. Carlin, *Inorg. Chem.* **28**, 272 (1989).
- [23] J. Villain, in *Proceedings of the 13th IUPAP Conference on Statistical Physics*, edited by D. Cabib, C. G. Kuper, and I. Riess, Annals of the Israel Physical Society (Hilger, Bristol, 1978), Vol. 2, p. 565.
- [24] J. C. Bonner and M. E. Fisher, *Phys. Rev.* **135**, A640 (1964).
- [25] Yu. Savina, O. Budlov, V. Pashchenko, S. L. Gnatchenko, P. Lemmens, and H. Berger, *Phys. Rev. B* **84**, 104447 (2011).
- [26] H. Lueken, *Magnetochemie: Eine Einfuehrung in Theorie und Anwendung* (Teubner Studienbuecher Chemie, Stuttgart-Leipzig, 1999).
- [27] N. W. Ashcroft and N. D. Mermin, *Solid State Physics* (Saunders College, Philadelphia, 1976).
- [28] A. Abragam, *Principles of Nuclear Magnetism* (Oxford University Press, New York, 1961).
- [29] P. Kunthia, M. Mariani, A. V. Mahajan, A. Lascialfari, F. Borsa, T. D. Pasatoiu, and M. Andruh, *Phys. Rev. B* **84**, 184439 (2011).
- [30] T. Moriya, *Prog. Theor. Phys.* **16**, 23 (1956); **28**, 371 (1962).
- [31] M. Steiner, J. Villain, and C. G. Windsor, *Adv. Phys.* **25**, 87 (1976).
- [32] H. Kawamura, *J. Phys.: Condens. Matter* **10**, 4707 (1998).
- [33] H. Schenck, V. L. Pokrovsky, and T. Nattermann, *Phys. Rev. Lett.* **112**, 157201 (2014).
- [34] S. V. Maleyev, *Phys. Usp.* **45**, 569 (2002).
- [35] V. P. Plakhty, W. Schweika, Th. Brückel, J. Kulda, S. V. Gavrillov, L.-P. Regnault, and D. Visser, *Phys. Rev. B* **64**, 100402(R) (2001).
- [36] T. Nagamiya, in *Solid State Physics*, edited by F. Seitz, D. Turnbull, and H. Ehrenreich (Academic Press, New York, 1967), Vol. 20, p. 306.
- [37] B. R. Cooper, in *Magnetic Properties of Rare Earth Metals*, edited by R. J. Elliot (Plenum, New York, 1972), p. 17.
- [38] T. Nagamiya and Y. Kitano, *Prog. Theoret. Phys.* **31**, 1 (1964).
- [39] T. Nagamiya, K. Nagata, and Y. Kitano, *Prog. Theoret. Phys.* **27**, 1253 (1962).
- [40] A. A. Gippius, A. S. Moskvin, and S.-L. Drechsler, *Phys. Rev. B* **77**, 180403(R) (2008).
- [41] P. C. Hohenberg and B. I. Halperin, *Rev. Mod. Phys.* **49**, 435 (1977).
- [42] E. H. Stanley, *Introduction to Phase Transitions and Critical Phenomena* (Oxford University Press, London, 1971).
- [43] M. Belesi, A. Lascialfari, D. Prociassi, Z. H. Jang, and F. Borsa, *Phys. Rev. B* **72**, 014440 (2005).
- [44] D. J. Scalapino, Y. Imry, and P. Pincus, *Phys. Rev. B* **11**, 2042 (1975).